CHEMISTRY
A European Journal

Supporting Information

Synthesis and Characterization of a Helicene-Based Imidazolium Salt and Its Application in Organic Molecular Electronics

Jan Storch,*[a] Jaroslav Zadny,[a] Tomas Strasak,[a] Martin Kubala,[b] Jan Sykora,[a] Michal Dusek,[c] Vladimir Cirkva,[a] Pavel Matejka,[d] Milos Krbal,[e] and Jan Vacek*[f]

chem_201405239_sm_miscellaneous_information.pdf

Content:

1. Introduction – Overview of Helicene Derivatives and Their Applications

Table S1: Methods, characterizations and applications of various [n]helicene derivatives.

Compound(s)	Characterized by Methods	Properties and Applications	Ref.
Ethylenedithio-tetrathiafulvalene-[4]helicene and [6]helicenes	UV/Vis spectrometry, X-ray diffraction analysis, cyclic voltammetry, CD spectroscopy, theoretical calculations	Redox active and chiroptical properties.	[1]
Helical polymers prepared by condensation of helicene *bis*-salicylaldehydes	MALDI-TOF, IR, UV and CD spectroscopy	Soluble polymers with ladder structure, chiroptical properties.	[2]
Pyrene-based [4]helicenes	UV/Vis absorption, cyclic voltammetry, H NMR,	Possible applications in optoelectronics.	[3]
Helical polymers of poly(thiaheterohrelicene)s	Magnetic circular dichroism, NMR, IR, UV/Vis spectrometry	Molecular-based electronic device was proposed.	[4]
Thiaheterohelicenes	Cyclic voltammetry, X-ray diffraction analysis, ESR spectroscopy	Possible chiral conducting materials, donor properties.	[5]
Azoniathiahelicenes and azoniadithia[6]helicenes	NMR	Possible applications in optoelectronics.	[6,7]
1,14-Dimethyl[5]helicene-spermine ligands	CD spectroscopy, surface plasmon resonance, NMR	Chiral recognition of B- and Z-DNA forms.	[8]
1,13-Dimethoxy-chromeno[2,3,4-*kl*]xanthenium hexafluorophosphate	MALDI-TOF, X-ray analysis, fluorescence spectroscopy	Helicenium dyes	[9]
Chromenoxanthene [4]helicene	X-ray diffraction analysis, CSP-HPLC, CD spectroscopy, NMR	Chirality of [4]helicene cation was shown.	[10]
4ª,14a-Diazoniaanthra[1,2-*a*]anthracene	X-ray diffraction analysis, NMR, MS and elemental analysis	Photopersistence and possible application in nucleic acid research was confirmed and proposed, respectively.	[11]
Monoaza[5]helicenes	NMR, theoretical calculations	Possible applications for optoelectronics.	[12]
2,15-Dihydroxy-hexahelicene	NMR, CD spectroscopy, fluorescence spectroscopy	High fluorescent intensity and possible use as an enantioselective sensor.	[13]

Hexaaza[5]helicene	NMR, X-ray diffraction analysis	Chiroptical properties, novel chiral materials.	[14]
Tetrathia[7]helicene, 2-formyl-tetrathia[7]helicene	NMR	Possible novel chiral materials.	[15]
Metal[7]helicene complexes	NMR	Molecular tweezer for a Ag(I) ion, chiroptical properties.	[16]
Dimethylsila[7]helicene	X-ray analysis, UV-vis spectroscopy, differential pulse voltammetry	High luminescence quantum yield, and characteristic chiroptics properties.	[17]

2. Synthesis, NMR and X-ray structure

^{1}H and $^{13}C\{^{1}H\}$ spectra were recorded using a 500 MHz Unity INOVA Varian instrument. Chemical shifts are reported in parts per million (δ) relative to TMS, referenced to the signal of $CDCl_3$ (δ 7.26 ppm and δ 77.00 ppm, respectively). The EI mass spectra were determined at an ionizing voltage of 70 eV, the *m/z* values are given along with their relative intensities (%). The standard 70 eV spectra were recorded in positive ion mode. The sample was dissolved in chloroform, loaded into a quartz cup of the direct probe and inserted into the ion source. The source temperature was 220 °C. For precise mass measurement, the spectra were internally calibrated using perfluorotri-*n*-butylamine (Heptacosa). The ESI mass spectra were recorded using a ZQ micromass mass spectrometer (Waters) equipped with an ESCi multi-mode ion source and controlled with MassLynx software. Diffraction data were collected at 120 K using a Gemini diffractometer (Oxford Diffraction) with the mirror monochromated Cu-Kα radiation. The IR spectra were measured in $CHCl_3$ (NICOLET 6700). TLC was performed on Silica gel 60 F_{254}-coated aluminium sheets and compounds were visualized with UV light (254 nm). Column chromatography was performed on a Biotage HPFC system with pre-packed flash silica gel columns. Commercially available reagent grade materials were used as obtained. 2-Methyl[6]helicene was purchased from Lach-ner s.r.o., Czech Republic. 1-Butyl-3-methyl imidazolium bromide was donated by Ionic Liquids Technologies GmbH (Heilbronn, DE).

2-Methyl[6]helicene (502.0 mg, 1.466 mmol), *N*-bromosuccinimide (417.5 mg, 2.346 mmol, 1.6 eq) and dibenzoylperoxide (48.7 mg, 0.201 mmol, 14 mol%) were dissolved in CCl_4 (100 mL) in a round-bottomed flask equipped with a condenser. The reaction mixture was heated to reflux overnight. The solvent was evaporated and the residue was purified by

flash chromatography on silica gel (petroleum ether:ether = 98:2) to give 2-bromomethyl[6]helicene **1** (368.2 mg, 60%) as a pale yellow powder.

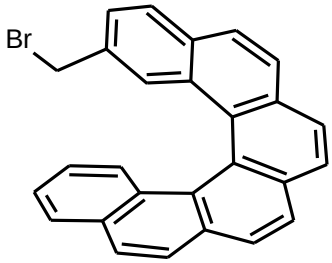

2-Bromomethyl[6]helicene **(1)**

^{1}H NMR (500 MHz, $CDCl_3$): δ 3.83 (d, *J* = 10.1 Hz, 1H), 3.96 (d, *J* = 10.1 Hz, 1H), 6.69 (ddd, *J* = 8.5, 6.9, 1.4 Hz, 1H), 7.29 – 7.20 (m, 1H), 7.56 (d, *J* = 8.6 Hz, 1H), 7.60 (s, 1H), 7.82 (d, *J* = 8.2 Hz, 1H), 7.84 (d, *J* = 7.9 Hz, 1H), 7.90 (d, *J* = 8.5 Hz, 1H), 7.93 – 8.05 (m, 8H) ppm. **^{13}C NMR (125 MHz, $CDCl_3$):** δ 33.79 (t), 123.99 (s), 124.69 (d), 125.78 (d), 126.12 (d), 126.26 (d), 126.96 (d), 126.99 (d), 127.20 (d), 127.23 (d), 127.41 (d), 127.42 (d), 127.64 (d), 127.66 (d), 127.70 (s), 127.74 (s), 127.95 (d), 128.25 (d), 128.30 (d), 129.64 (s), 129.66 (s), 131.40 (s), 131.44 (s), 131.52 (s), 131.88 (s), 133.19 (s), 134.11 (s) ppm. **IR ($CHCl_3$):** 3051 w, 3088 vw sh, 2928 w, 2855 w, 1439 w, 1605 w, 1582 vw, 1522 w, 1507 w, 1439 w, 1430 w, 1375 w, 1275 w, 1229 w, 1078 w, 1046 w, 1036 w, 1004 w, 950 w, 907 w, 868 w, 851 s, 823 w, 626 w, 613 m, 493 w, 479 w, 428 w, 422 w cm^{-1}. **EI MS:** 422 (31), 420 (31), 356 (7), 341 (100), 326 (85), 313 (16), 300 (58), 287 (7), 169 (12), 162 (18), 150 (7), 143 (5), 82 (19), 80 (19), 73 (8), 60 (11), 57 (22), 55 (21). **HR EI MS:** calculated for $C_{27}H_{17}Br$ 420.0514, found 420.0518.

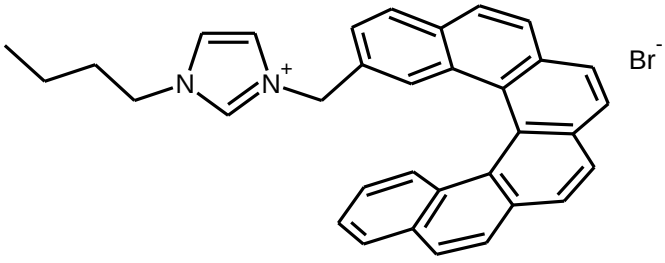

1-Butyl-3-(2-methyl[6]helicenyl)-imidazolium bromide **(2)**

2-Bromomethyl[6]helicene **1** (200 mg, 0.475 mmol) and 1-butylimidazole (187 ml, 176 mg, 1.425 mmol, 3.0 eq) were stirred in methylisobutyl ketone (10 mL) at 90 °C

overnight. The solid was filtered off, washed with petroleum ether and dried under vacuum to give 1-butyl-3-(2-methyl[6]helicenyl)-imidazolium bromide **2** (206 mg, 80%) as a pale yellow amorphous solid.

^{1}H NMR (500 MHz, $CDCl_3$): δ 0.90 (t, *J* = 7.4 Hz, 3H), 1.30 (h, *J* = 7.4 Hz, 2H), 1.82 (p, *J* = 7.6 Hz, 2H), 4.24 (t, *J* = 7.4 Hz, 2H), 4.58 (d, *J* = 14.4 Hz, 1H), 5.10 (d, *J* = 14.4 Hz, 1H), 5.89 (dd, *J* = 1.8, 1.8 Hz, 1H), 6.67 (ddd, *J* = 8.4, 6.9, 1.4 Hz, 1H), 7.20 (m, 2H), 7.51 (bs, 1H), 7.55 (d, *J* = 8.6 Hz, 1H), 7.78 (d, *J* = 8.2 Hz, 1H), 7.82 (m, 1H), 7.85 (d, *J* = 8.7 Hz, 1H), 7.88 – 8.01 (m, 8H), 10.39 (s, 1H) ppm. **^{13}C NMR (125 MHz, $CDCl_3$):** δ 13.39 (q), 19.40 (t), 32.00 (t), 49.77 (t), 53.09 (t), 121.22 (s), 121.70 (s), 123.52 (s), 124.97 (d), 125.29 (d), 125.78 (d), 126.78 (d), 127.17 (d), 127.30 (d), 127.40 (d), 127.41 (d), 127.45 (d), 127.47 (s), 127.50 (d), 127.56 (d), 127.66 (d), 127.74 (d), 127.82 (d), 128.18 (d), 128.82 (d), 129.37 (d), 129.62 (s), 129.63 (s), 131.49 (s), 131.54 (s), 131.69 (s), 131.81 (s), 133.26 (s), 136.81 (d) ppm. **IR ($CHCl_3$):** 3143 w, 3167 w, 3031 w, 2959 vs, 2940 vs, 2878 m, 2833 w sh, 2709 w, 1617 w, 1605 w, 1585 w, 1556 m, 1522 vw, 1507 w, 1466 m, 1477 w, 1430 w, 1361 w, 1399 w, 1383 w, 1158 m, 1118 w, 1077 w, 1037 w, 1007 w, 951 w, 914 w sh, 852 s, 824 w, 662 m, 479 w, 428 w cm^{-1}. **ESI MS:** 465 ($[M^+]$). **HR ESI MS:** calculated for $C_{34}H_{29}N_2$ 465.23253, found 465.23261.

Crystallographic data: X-ray of comp. **2**: $C_{34}H_{29}N_2Br_1$, M = 545.5 g mol^{-1}, orthorhombic system, space group *Pbca*, a = 9.6540(1), b = 15.9235(1), c = 34.3397(3) Å, Z = 8, V = 5278.91(8) $Å^3$, Dc = 1.37 g cm^{-3}, μ(Cu Kα) = 2.31 mm^{-1}, T = 120 K, crystal dimensions of 0.3 x 0.1 x 0.1 mm. The structure was solved by direct methods (SHELXL97) [18] and refined by full-matrix least-squares on the F^2 values (CRYSTALS) [19]. All heavy atoms were refined anisotropically. Hydrogen atoms were localized from the expected geometry and most of them were refined isotropically; except for the hydrogen atoms located on the butyl side chain. The structure converged to a final R = 0.0317 and R_w = 0.0338 using 4472 independent reflections (θ_{max}=67.08°). The crystallographic data for the structure reported in this paper have been deposited in the Cambridge Crystallographic Data Centre as a supplementary publication. Copies of the data can be obtained free of charge by applying to CCDC, e-mail: deposit@ccdc.cam.ac.uk. CCDC registration number 963865.

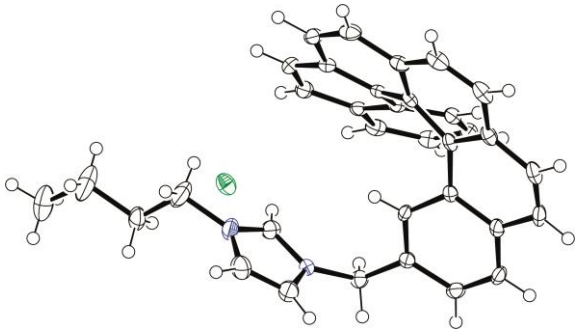

Fig. S1: ORTEP projection of **2**.

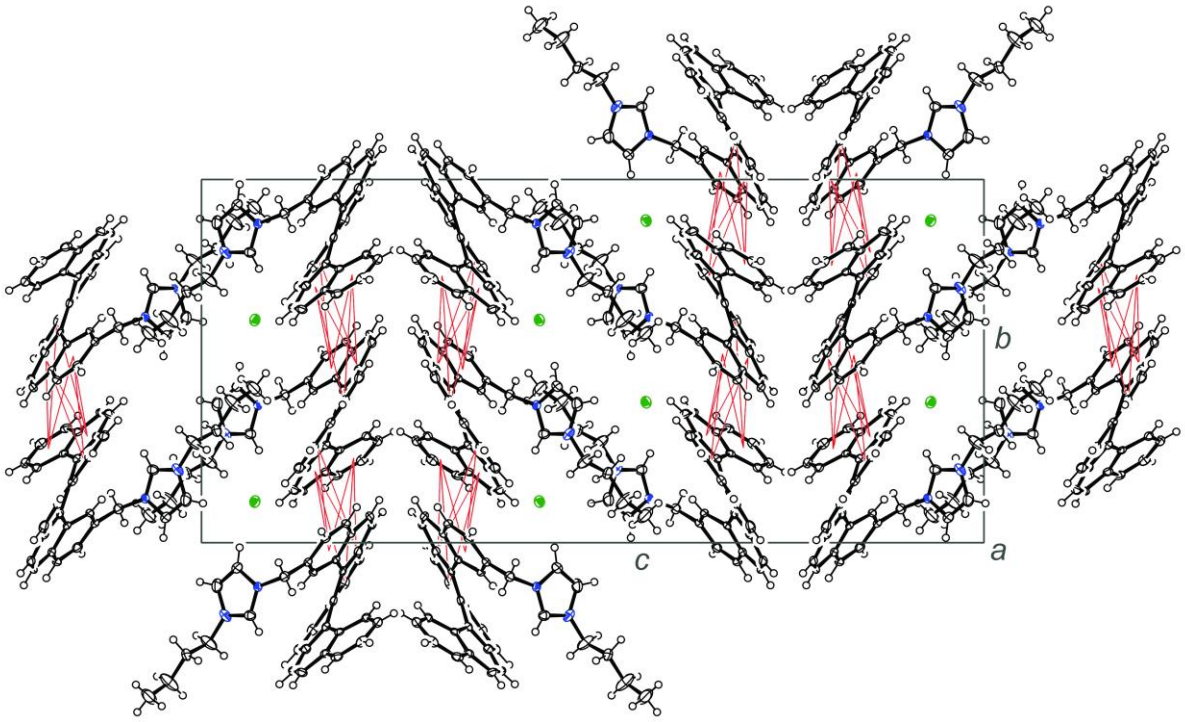

Fig. S2: ORTEP projection of molecular packing in the crystal structure of **2**.

3. Quantum-Chemical Calculations

All calculations were performed with the package Gaussian03 [20] with the B3LYP [21,22] hybrid functional and a 6-31G(d,p) basis set. In the DFT calculations the chloroform solvent was simulated with the polarizable continuum model (PCM). The natural bond orbital (NBO) calculation, performed at the same level of the theory, gave atomic charges through natural population analysis (NPA) using the NBO 3.1 program [23] included in the Gaussian 03. The vibrational analysis showed that all structures correspond to the local minima in the potential energy surface.

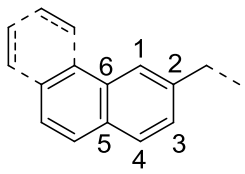

Table S2: Atomic charges through natural population analysis (NPA).

	C1	C2	C3	C4	C5	C6
Comp. **2**	−0.183	−0.087	−0.233	−0.203	−0.060	−0.040
2-Methyl[6]helicene	−0.202	−0.043	−0.235	−0.214	−0.079	−0.024

(NPA) were calculated using the B3LYP/6-31+G (d,p) method with the IEFPCM of chloroform.

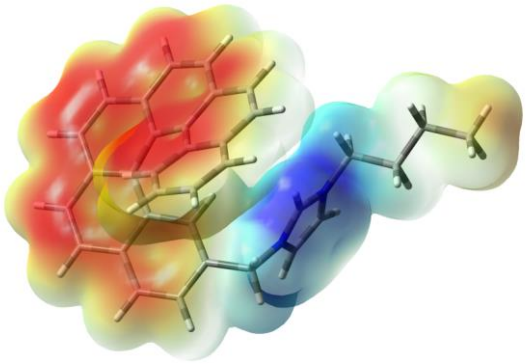

Fig. S3: Electron density isosurface mapped with electrostatic potential surface of **2** in the range from 0.06 (red) to 0.20 (blue).

4. Spectral Characterization and Transmission Spectroscopy

For comparing the effect of the imidazolium moiety on the optical and other physico-chemical properties of **2,** 1-butyl-3-methyl imidazolium bromide **3** was used for optical spectroscopy experiments:

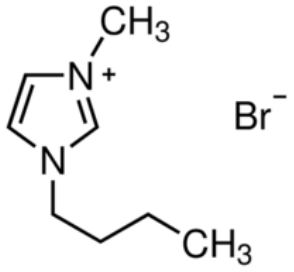

1-butyl-3-methyl imidazolium bromide **3**

Absorption spectra. Absorption spectra of solutions of 37 μM **2** or 300 μM **3** in chloroform were recorded on a Specord 250 spectrometer (Jena Bioscience, Germany) in a quartz cuvette with 1-cm optical path, using a pure solvent as a reference. The spectra were measured in the 250–800 nm interval, with a step of 0.5 nm, 1-nm bandpass, and a scan speed of 2 nm/s. The extinction coefficient ε(λ) was calculated from the formula:

$$\varepsilon(\lambda) = \frac{A(\lambda)}{c.l}$$

where $A(\lambda)$ is the estimated absorbance, c is the sample concentration and l is the optical path.

Steady-state fluorescence spectra. Steady-state excitation and emission spectra of 1.6 μM **2** or 30 μM **3** in chloroform were recorded using F-4500 fluorometer (Hitachi, Japan) in a quartz cuvette with a 1-cm optical path (for both excitation and emission). Hence, the absorbance of the sample at the excitation wavelength should be below 0.05 in all cases, and therefore the inner-filter effect could be neglected. Bandpasses in both the excitation and emission monochromator were set to 5 nm, the spectra were scanned with a 15 nm/min speed at 22°C. Emission spectra of **3** were recorded with excitation at 274 nm and those of **2** with excitation at 318 nm, 328 nm or 350 nm.

Quantum yield (QY) estimation. The emission spectra of 1.6 μM **2** in chloroform and of 11 μM anthracene in ethanol, were acquired under the conditions described in the above paragraph. The fluorescence intensity was integrated in the 360–600 nm interval, and the quantum yield *QY* was calculated from the formula:

$$QY = \frac{A_S}{A}\frac{F}{F_S}\frac{n^2}{n_S^2}QY_S$$

where *A*, *F* and *n* refer to the absorbance at the excitation wavelength, integrated fluorescence intensity and refractive index, respectively, the subscript *S* refers to the standard (anthracene in ethanol, $QY_S = 0.28 \pm 0.02$, [24]). The absorbance of both **2** and anthracene was determined experimentally, using the pure solvent as a reference.

Time-resolved fluorescence measurements. Fluorescence decays of 5 μM **2** solutions in chloroform were measured on a PicoHarp300 TCSPC fluorometer (Picoquant, Germany),

using a pulsed LED centered at 308 nm (the best excitation wavelength available) as the source of excitation light and operated at 10 MHz and maximum intensity. Data were plotted as a histogram on the time-scale 0–100 ns, where the time-width of one channel was 32 ps. The instrument response function (IRF) was obtained using Ludox solution as a scatterer, the estimated FWHM(IRF) was 0.48 ns. Emission was detected under magic-angle conditions at 442 nm, the emission bandpass was 16 nm. The data were acquired at 22 °C for 300 s. Fluorescence decay was fitted using the software FluoFit 4.2.1 (PicoQuant), and could be adequately fitted to the 1-exponential model with IRF deconvolution, with χ_R^2 close to 1.00 and a random distribution of residuals. Standard error (68% confidence interval) of the fluorescence lifetime was determined using the support plane analysis (SPA) method. The rates for radiative (k_R) and non-radiative (k_N) deexcitation processes were calculated from the quantum yield (QY) and fluorescence lifetime (τ) using the formulae:

$$k_R = \frac{QY}{\tau}$$

and

$$k_N = \frac{1-QY}{\tau}$$

Transmission spectra. The optical transmission spectra of the films were recorded with a Jasco V-570 UV/VIS/NIR spectrophotometer. The spectra were measured in two spectral regions: 190–900 nm with a step of 2 nm and 900–2000nm with a step of 8 nm.

Raman spectra. The Raman spectroscopic study was performed on a Fourier transformation (FT) Raman spectrometer (Bruker, model IFS/FRA 106, Germany). Raman spectra were excited using a laser beam with λ = 1064 nm having an output power of 90 mW. The resolution of the Raman spectrometer was set at 1 cm^{-1}.

5. Spincoating, Conductivity Measurement and Cell Construction

Thin films were deposited by spincoating (1000 rps for 40 s) with a thickness of about 300 nm onto silica glass substrates from a 15 $mg.ml^{-1}$ solution of **2** in chloroform. The device sizes were 1 cm × 1 cm (length × width). Annealing conditions were 100 °C for 30 min at 2

Pa and an Ar atmosphere in order to remove the solvent completely after the deposition. Gold contacts (~130nm) were deposited using the thermal evaporation technique.

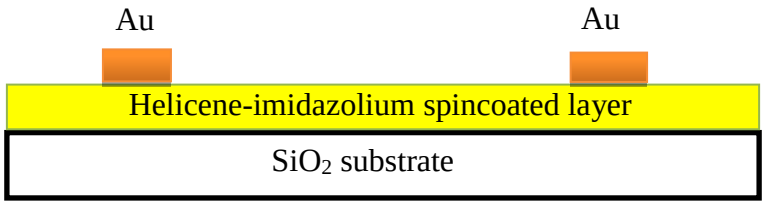

Fig. S4: Schematic representation of the designed cell. SiO_2 substrate/spincoated **2** (thickness 300nm)/Au (thickness 130 nm and the spacing between electrodes was 1cm).

The electrical performance of spincoated **2** samples was measured using a complex setup consisting of an optical microscope (Süss Microtec PSM 1000) mounted on a manual probe system (Süss Microtec PM 5) equipped with microcontrolers (Süss Microtec pH 100) holding gold-plated tungsten tips (American probe and technologies, Inc model 72G-F3/250x1.25) in contact with the measurement unit (Keithley 2602 System SourceMeter). The probes were placed on the Au electrodes. The Keithley 2602 System SourceMeter was controlled by computer via a script written in the software Test Script Builder (version KTS-850E02). Cyclic voltammograms (CVs) were obtained after applying a set of pulses. For the cell, the voltage was swept from 0 V to 28 V, then to −28 V and back to 0 V. The pulse voltage was changed in steps of 0.05 V and the pulse duration was 100 ms, individual pulses were separated with a 100 ms delay. The conductivity dependence on temperature was measured using a heating cell (THMSG 600) over the temperature range 20–160 °C at ambient conditions and 2 Pa (rotary vacuum pump) under a constant flow of inert gas (Ar). In this experiment, thin copper wire contacts were fixed to the Au electrodes with a graphite paste to ensure the best conductivity.

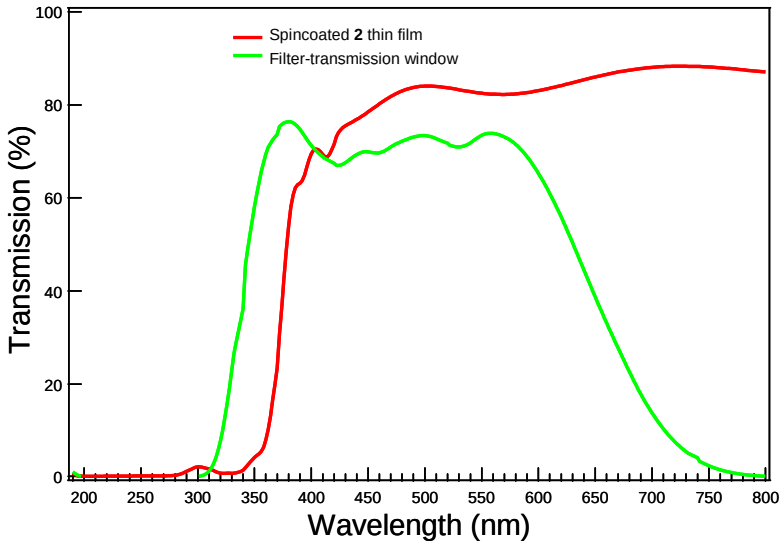

Fig. S5: Transmission spectrum of thin film of 2 annealed at 100 °C on SiO_2 substrate (red line) and transmission window of filter used for light exposure experiments (green line). We applied the filter to cut off the IR spectrum of the polychromatic light source to prevent additional heating of the sample. For other details, see Section 4.

References

(1) Biet, T.; Fihey, A.; Cauchy, T.; Vanthuyne, N.; Roussel, C.; Crassous, J.; Avarvari, N. *Chem. Eur. J.* **2013**, *19*, 13160.

(2) Dai, Y.; Katz, T. J. *J. Org. Chem.* **1997**, *62*, 1274.

(3) Hu, J. Y.; Feng, X.; Paudel, A.; Tomiyasu, H.; Rayhan, U.; Thuery, P.; Elsegood, M. R. J.; Redshaw, C.; Yamato, T. *Eur. J. Org. Chem.* **2013**, 5829.

(4) Iwasaki, T.; Katayose, K.; Kohinata, Y.; Nishide, H. *Polym. J.* **2005**, *37*, 592.

(5) Larsen, J.; Dolbecq, A.; Bechgaard, K. *Acta Chem. Scand.* **1996**, *50*, 83.

(6) Sato, K.; Katayama, Y.; Yamagishi, T.; Arai, S. *J. Heterocyclic Chem.* **2006**, *43*, 177.

(7) Sato, K.; Okazaki, S.; Yamagishi, T.; Arai, S. *J. Heterocyclic Chem.* **2004**, *41*, 443.

(8) Tsuji, G.; Kawakami, K.; Sasaki, S. *Bioorg. Med. Chem.* **2013**, *21*, 6063.

(9) Sørensen, T. J.; Madsen, A. Ø.; Laursen, B. W. *Tetrahedron Lett.* **2013**, *54*, 587.

(10) Guin, J.; Besnard, C. l.; Lacour, J. r. m. *Org. Lett.* **2010**, *12*, 1748.

(11) Granzhan, A.; Bats, J. W.; Ihmels, H. *Synthesis* **2006**, *2006*, 1549.

(12) Abbate, S.; Bazzini, C.; Caronna, T.; Fontana, F.; Gambarotti, C.; Gangemi, F.; Longhi, G.; Mele, A.; Sora, I. N.; Panzeri, W. *Tetrahedron* **2006**, *62*, 139.

(13) Reetz, M. T.; Sostmann, S. *Tetrahedron* **2001**, *57*, 2515.

(14) Adam, R.; Ballesteros-Garrido, R.; Vallcorba, O.; Abarca, B.; Ballesteros, R.; Leroux, F. R.; Colobert, F.; Amigó, J. M.; Rius, J. *Tetrahedron Lett.* **2013**, *54*, 4316.

(15) Maiorana, S.; Papagni, A.; Licandro, E.; Annunziata, R.; Paravidino, P.; Perdicchia, D.; Giannini, C.; Bencini, M.; Clays, K.; Persoons, A. *Tetrahedron* **2003**, *59*, 6481.

(16) Fuchter, M. J.; Schaefer, J.; Judge, D. K.; Wardzinski, B.; Weimar, M.; Krossing, I. *Dalton Trans.* **2012**, *41*, 8238.

(17) Oyama, H.; Nakano, K.; Harada, T.; Kuroda, R.; Naito, M.; Nobusawa, K.; Nozaki, K. *Org. Lett.* **2013**, *15*, 2104.

(18) Sheldrick, G. M. *SHELXL97. Program for Crystal Structure Refinement from Diffraction Data, University of Göttingen, Göttingen* **1997**.

(19) Betteridge, P. W.; Carruthers, J. R.; Cooper, R. I.; Prout, K.; Watkin, D. J. *J. Appl. Crystallogr.* **2003**, *36*, 1487.

(20) Frisch, M. J.; Trucks, G. W.; Schlegel, H. B.; Scuseria, G. E.; Robb, M. A.; Chesseman, J. R.; Zakrzewski, V. G.; Montgomery Jr., J. A.; Stratmann, R. E.; Burant, J. C.; Dapprich, S.; Millam, J. M.; Daniels, A. D.; Kudin, K. N.; Strain, M. C.; Farkas, O.; Tomasi, J.; Barone, V.; Cossi, M.; Cammi, R.; Mennucci, B.; Pomelli, C.; Adamo, C.; Clifford, S.; Ochterski, J.; Petersson, G. A.; Ayala, P. Y.; Cui, Q.; Morokuma, K.; Malick, D. K.; Rabuck, A. D.; Raghavachari, K.; Forseman, J. B.; Cioslowski, J.; Ortiz, J. V.; Baboul, A. G.; Stefanov, B. B.; Liu, G.; Liashenko, A.; Piskorz, P.; Komaromi, I.; Gomperts, R.; Martin, R. L.; Fox, D. J.; Keith, T.; AlLoham, M. A.; Peng, C. Y.; Nanayakkara, A.; Gonzalez, C.; Challacombe, M.; Gill, P. M. W.; Johnson, B. G.; Chen, W.; Wong, M. W.; Andres, J. L.; Head-Gordon, M.; Replogle, E. S.; Pople, J. A. *Gaussian 03; Gaussian Inc.: Wallingford, CT* **2003**.

(21) Becke, A. D. *J. Chem. Phys.* **1993**, *98*, 5648.

(22) Lee, C. T.; Yang, W. T.; Parr, R. G. *Phys. Rev. B* **1988**, *37*, 785.

(23) Glendening, E. D.; Reed, A. E.; Carpenter, J. E.; Weinhod, F. *NBO Version 3.1, TCI, University of Wisconsion*.

(24) (a) Brouwer, A. M. *Pure Appl. Chem.* **2011**, *83*, 2213(b) Suzuki, K.; Kobayashi, A.; Kaneko, S.; Takehira, K.; Yoshihara, T.; Ishida, H.; Shiina, Y.; Oishic, S.; Tobita, S. *Phys. Chem. Chem. Phys.* **2009**, *11*, 9850.